

A kilobyte rewritable atomic memory

F. E. Kalff¹, M. P. Rebergen¹, E. Fahrenfort¹, J. Girovsky¹, R. Toskovic¹, J. L. Lado², J. Fernández-Rossier^{2,3} and A. F. Otte^{1*}

The advent of devices based on single dopants, such as the single-atom transistor¹, the single-spin magnetometer^{2,3} and the single-atom memory⁴, has motivated the quest for strategies that permit the control of matter with atomic precision. Manipulation of individual atoms by low-temperature scanning tunnelling microscopy⁵ provides ways to store data in atoms, encoded either into their charge state^{6,7}, magnetization state^{8–10} or lattice position¹¹. A clear challenge now is the controlled integration of these individual functional atoms into extended, scalable atomic circuits. Here, we present a robust digital atomic-scale memory of up to 1 kilobyte (8,000 bits) using an array of individual surface vacancies in a chlorine-terminated Cu(100) surface. The memory can be read and rewritten automatically by means of atomic-scale markers and offers an areal density of 502 terabits per square inch, outperforming state-of-the-art hard disk drives by three orders of magnitude. Furthermore, the chlorine vacancies are found to be stable at temperatures up to 77 K, offering the potential for expanding large-scale atomic assembly towards ambient conditions.

Since the first demonstration of atom manipulation, 25 years ago⁵, the preferred approach for assembling atomic arrangements has been the lateral positioning of atoms or molecules evaporated onto a flat metal surface, most notably the (111) crystal surface of copper^{12–15}. Although ideal for experiments comprising up to several hundreds of constituents, the absence of a large-scale defect-free detectable grid on this surface prohibits the construction of architectures involving correlated lattice-placement of atoms separated by more than a few nanometres. Moreover, thermal motion of the adatoms restricts the technique to temperatures below 10 K. As we demonstrate in the following, we find that manipulation of missing atoms in a surface (vacancies)^{16–18}, as opposed to additional atoms on top, permits a profound advance in our capability to build functional devices on the atomic scale.

For this purpose, we take advantage of the self-assembly of chlorine atoms on the Cu(100) surface^{19–22}, forming a flat two-dimensional lattice with several convenient properties. First, it provides large areas of a perfect template grid, with a controllable coverage of vacancies. Second, the chlorine lattice remains stable up to a large density of vacancies and up to a relatively high temperature (77 K). Third—and critical for our purpose—the precise location of the vacancies can be manipulated by scanning tunnelling microscopy (STM) with a very high level of control (and without the need to pick up atoms with the tip; that is, vertical atom manipulation). As we show, these properties allow us to position thousands of vacancies at predefined atomic sites in a reasonable timeframe. Comparably large atomic-scale data storage has been demonstrated before using individual Si atoms on top of a Si–Au surface¹¹, but, in contrast to the current work, the memory could be written only once, and the entire surface had to be regenerated to change a single bit.

The chlorinated copper surface was prepared in ultrahigh vacuum through the evaporation of anhydrous CuCl₂ powder heated to 300 °C onto a clean Cu(100) crystal surface. The crystal was pre-heated to 100–150 °C before CuCl₂ deposition for ~12 min and kept at this temperature during the deposition and the 10 min post-anneal. This resulted in the formation of a square $c(2 \times 2)$ reconstruction of Cl atoms with a lattice constant a of 0.36 nm. The Cl coverage (and therefore the vacancy coverage x) depends on the duration of evaporation. For most of the results presented here we used an evaporation time of 210 s, resulting in a vacancy coverage of $x = 0.115$ (see Methods for details).

When imaged by STM, vacancies are resolved as square depressions ~20–30 pm deep (Fig. 1). According to density functional theory (DFT) calculations (see Methods), a Cl atom has to overcome an energy barrier of $\Delta = 0.3$ eV in order to swap places with a neighbouring vacancy (Fig. 1a,b). As a result, the surface is resilient to tunnelling currents of up to 2 μA when imaged at positive sample voltages of ~200 mV or lower.

As shown in Fig. 1c,d, vacancies can be moved by injecting a current of 1.0 ± 0.5 μA (error represents variations from tip to tip in the exact shape of the STM tip apex) at +500 mV sample voltage at a position $\sim 0.4a$ along the way from the centre of the vacancy to the centre of the neighbouring Cl atom at the desired location. The STM feedback is kept switched on throughout the manipulation procedure. Although several attempts may be required to make a vacancy move, the directional reliability (that is, how often a vacancy moves in the desired direction once it moves) can be in excess of 99%, depending on the tip shape. Controlled vacancy movement is limited to the $(\pm 1, 0)$ and $(0, \pm 1)$ directions on the square Cl grid. Diagonal moves (for example, in the $(1, 1)$ direction) were found to occur sporadically, but could not be induced controllably. See Supplementary Section 1 for a discussion on the manipulation mechanism.

In our structure, we define a pair consisting of a chlorine atom (Cl) and a vacancy (V) as a bit, where the V–Cl configuration (as read from top to bottom in the STM scans) represents the ‘0’ and Cl–V the ‘1’. To avoid vacancies directly neighbouring each other, which would render automated locking of the STM tip on individual vacancies impossible, we implemented a row of Cl atoms to separate bits in both the horizontal and vertical directions. For this reason, six lattice sites are needed for a bit, or 48 lattice sites for a byte (Fig. 2a), resulting in an optimal vacancy coverage of $x = 1/6 = 0.167$.

We have not been able to controllably create or destroy vacancies without altering the tip apex. As a result, the vacancy coverage can be controlled only during sample preparation and cannot be changed afterwards. The bit arrays presented here were all made on a surface with $x = 0.115$. To compensate for the vacancy deficiency in comparison to the optimal coverage, the memory is organized into blocks of 8 bytes (64 bits) as shown in Fig. 2b–d, separated by a margin of four unit cells. Constructing this block

¹Department of Quantum Nanoscience, Kavli Institute of Nanoscience, Delft University of Technology, Lorentzweg 1, 2628 CJ Delft, The Netherlands.

²International Iberian Nanotechnology Laboratory (INL), Avenida Mestre José Veiga, 4715-310 Braga, Portugal. ³Departamento de Física Aplicada, Universidad de Alicante, San Vicente del Raspeig 03690, Spain. *e-mail: a.f.otte@tudelft.nl

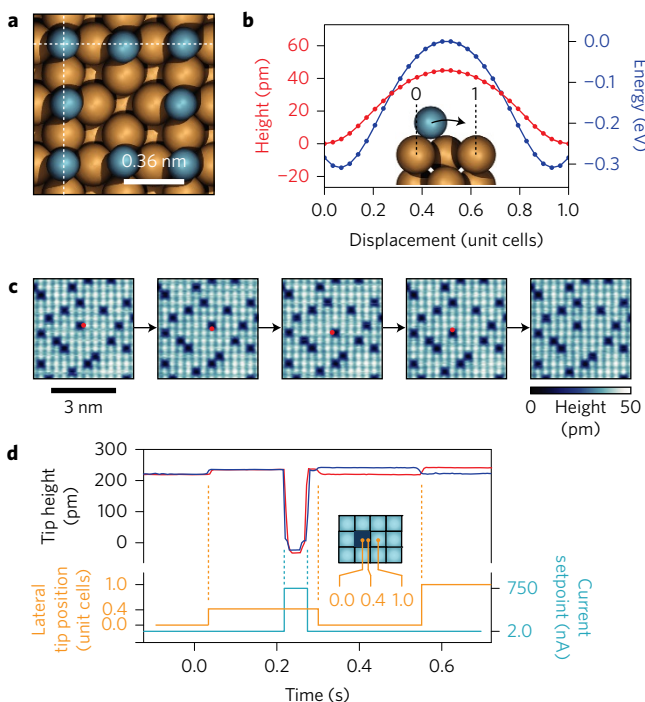


Figure 1 | Hopping mechanism of a Cl vacancy on chlorinated Cu(100). **a**, Atomic structure around a vacancy, calculated by DFT. Cl atoms (blue) are found to relax slightly towards the centre of the vacancy with respect to their original locations (dashed lines). **b**, DFT calculations provide the height profile and the corresponding potential energy of a Cl atom during a switch. **c**, Consecutive STM images (tunnelling current $I = 2.00$ nA, sample bias voltage $V = +500$ mV, temperature $T = 1.5$ K) of a vacancy being hopped in all four directions. The tip position for each manipulation is designated by a red dot. **d**, Measured tip height during a successful (blue) and an unsuccessful (red) manipulation. Yellow and cyan curves show the lateral tip position (see inset) and applied tunnelling current setpoint, respectively. $V = +500$ mV throughout the manipulation. After the manipulation, the tip visits the original location of the Cl atom and the target position. Variations in the tip height between these two positions indicate whether the manipulation has been successful.

configuration requires a vacancy coverage of $x = 0.118$, which is within 3% of the actual coverage. These blocks form a convenient way to organize the data. A readout and a rewrite of a block take ~1 and 2 min, respectively.

We make use of an autonomous manipulation method²³ (see Methods) that permits the construction of large memories. A marker at the top left of each block defines the scan frame and the lattice for the complete block. After scanning the area, the positions of all vacancies are determined via image recognition. Next, a pathfinding algorithm is used to calculate the building sequence, guiding the vacancies to their respective final positions. The markers for adjacent blocks are built automatically as part of the construction, and leftover vacancies are swept to the side to be used in future blocks. Automated construction of a complete block takes on the order of 10 min (Supplementary Movie 1).

The scalability of the technique is demonstrated in Fig. 3 and Supplementary Fig. 1, which show a complete memory consisting of 1,016 bytes (8,128 atomic bits) written to two different texts. Owing to local defects or contaminants, some areas are not suitable for building switchable bits. Such local imperfections do not need to affect the functionality of the memory. By properly defining markers consisting of several vacancies, blocks can be designated as broken and will be skipped in the reading and writing sequences. Additional markers, denoting, for example, the start or end of a line,

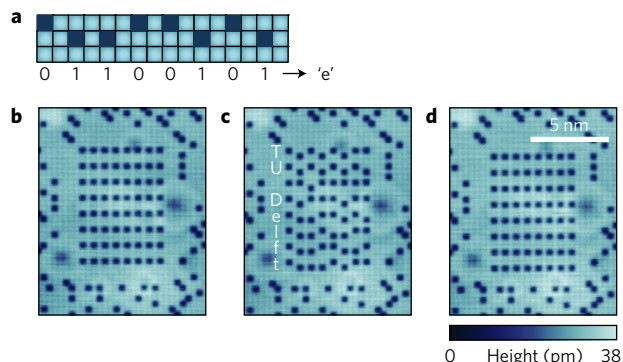


Figure 2 | Data-encoding principle. **a**, Diagram showing the smallest possible byte, provided that vacancies are not direct neighbours. The byte is set to represent the binary ASCII code for the character 'e'. **b-d**, STM images ($I = 2.00$ nA, $V = +500$ mV, $T = 1.5$ K) of a 64-bit block, written as all Os (**b**), a text (**c**) and all 1s (**d**).

allow for fully automated navigation of the STM tip through the memory. More complex markers may be designed to allow travel of the STM tip over longer distances and in arbitrary directions. Because 12% of blocks are not suitable for data storage, the actual areal density of the complete memory decreases to 0.778 bits nm^{-2} , or 502 terabits per square inch.

Our DFT calculations permit an order of magnitude estimate of the single-vacancy switching rates. The estimated attempt frequency for a Cl atom to overcome the energy barrier $\Delta = 0.3$ eV, obtained for the small oscillation analysis around the equilibrium position, yields $T_0 = 48$ THz. Thus, we can estimate the thermally activated switching rate $T_0 \exp(-\Delta/k_B T)$, where k_B is the Boltzmann constant, to be in the range of 1×10^{-5} Hz (several hours lifetime) at a temperature $T = 77$ K, although large error bars have to be assigned due to the exponential dependence on Δ . As shown in Fig. 4a and Fig. 4b, taken 44 h apart at 77.5 K, the manipulated vacancies are found experimentally to be stable for at least that amount of time, provided they are properly positioned. Vacancies arranged within two unit cells of each other are found to settle into a lower energy state within tens of minutes at this temperature (Supplementary Fig. 2).

To understand the vacancy–vacancy interaction, we computed several configurations with two vacancies (Fig. 4c) in a supercell of up to 5×5 Cl atoms. We find that the minimal energy configuration for a pair is the diagonal dimer, that is, two consecutive vacancies along the $(1,\pm 1)$ direction, which explains the observed high natural abundance of these. This finding goes a long way to account for the formation of a stripe phase with coexisting domains along the $(1,\pm 1)$ directions, observed near $x = 1/3$ (Fig. 4d). Monte Carlo simulations (see Methods), using the vacancy–vacancy interactions discussed above (Fig. 4e), are in very good agreement with the experiment and show that this system provides an ideal physical realization of a lattice gas model, for which stripe phases are expected²⁴.

Having several thousands of single-atom bits represents a significant step forward in the field of atomic-scale electronics. An important improvement still to be made is an increase in the readout speed. To this end, the memory would have to be scanned in constant height mode rather than constant current mode. At constant tip height, using settings similar to those presented here, the current difference between a Cl atom and a vacancy is on the order of 1 nA. Demonstrated high-frequency STM electronics²⁵ allow a 1 nA signal to be measured at a bandwidth of 1 MHz, suggesting that readout speeds on the order of 1 Mb s^{-1} should be attainable. The required scan speed of 0.36 mm s^{-1} can be achieved by using video-rate STM²⁵. There is no physical limitation that prevents the fabrication of much larger in-plane atomic memories.

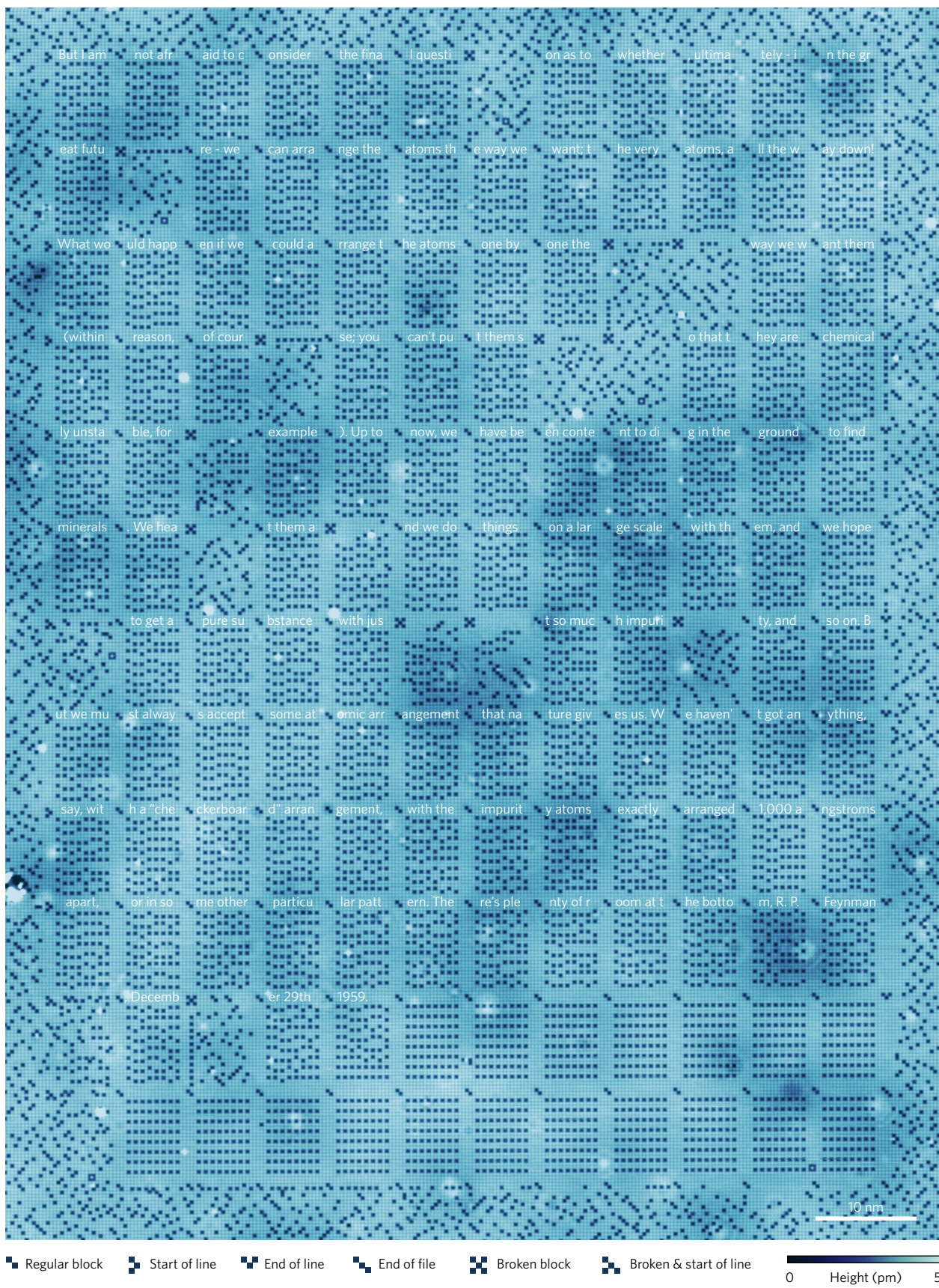


Figure 3 | Kilobyte atomic memory. STM image (96×126 nm, $I = 2.00$ nA, $V = +500$ mV, $T = 1.5$ K) of a 1,016-byte atomic memory, written to a passage from Feynman's lecture 'There's plenty of room at the bottom'²⁶. The various markers used are explained in the legend below the images. The memory consists of 127 functional blocks and 17 broken blocks, resulting in an overall areal density of 0.778 bits nm $^{-2}$.

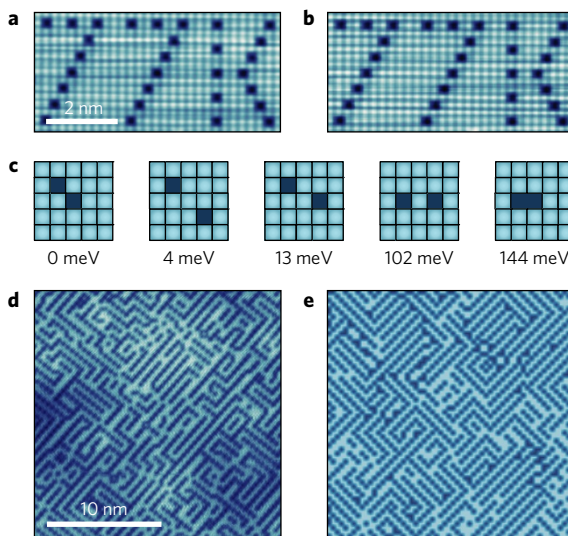


Figure 4 | Thermal stability and vacancy–vacancy interactions.

a, STM image ($I = 300$ pA, $V = +200$ mV) of arranged vacancies measured at 77.5 K. **b**, As in **a**, but taken 44 h later. **c**, DFT calculations on the energetics of pairs of vacancies, indicating that orientations along the (1,1) direction are strongly favoured over orientations along the (1,0) direction. **d**, STM image ($I = 500$ pA, $V = +500$ mV, $T = 1.5$ K) taken at a vacancy coverage of $x = 0.309$, showing a stripe pattern. **e**, Monte Carlo simulation for $T = 100$ K of a two-dimensional vacancy gas with $x = 1/3$ and vacancy–vacancy interactions as shown in **c**. The cell size is 60×60 , and the result is shown after 400,000 steps starting from a random distribution.

Translating the two-dimensional storage density presented here to three dimensions, would—assuming a modest vertical pitch of 5 nm—allow the storage of the entire US Library of Congress in a cube 100 μm wide.

Methods

Methods and any associated references are available in the [online version of the paper](#).

Received 17 March 2016; accepted 15 June 2016;
published online 18 July 2016

References

- Fuechsle, M. *et al.* Spectroscopy of few-electron single-crystal silicon quantum dots. *Nature Nanotech.* **5**, 502–505 (2010).
- Maze, J. R. *et al.* Nanoscale magnetic sensing with an individual electronic spin in diamond. *Nature* **455**, 644–647 (2008).
- Balasubramanian, G. *et al.* Nanoscale imaging magnetometry with diamond spins under ambient conditions. *Nature* **455**, 648–651 (2008).
- Schirm, C. *et al.* A current-driven single-atom memory. *Nature Nanotech.* **8**, 645–648 (2013).
- Eigler, D. M. & Schweizer, E. K. Positioning single atoms with a scanning tunnelling microscope. *Nature* **344**, 524–526 (1990).
- Repp, J., Meyer, G., Olsson, F. E. & Persson, M. Controlling the charge state of individual gold adatoms. *Science* **305**, 493–495 (2004).
- Eom, D., Moon, C.-Y. & Koo, J.-Y. Switching the charge state of individual surface atoms at Si(111)- $\sqrt{3} \times \sqrt{3}$:B surfaces. *Nano Lett.* **15**, 398–402 (2015).
- Loth, S., Baumann, S., Lutz, C. P., Eigler, D. M. & Heinrich, A. J. Bistability in atomic-scale antiferromagnets. *Science* **335**, 196–199 (2012).
- Khajetoorians, A. A. *et al.* Current-driven spin dynamics of artificially constructed quantum magnets. *Science* **339**, 55–59 (2013).
- Spinelli, A., Bryant, B., Delgado, F., Fernández-Rossier, J. & Otte, A. F. Imaging of spin waves in atomically designed nanomagnets. *Nature Mater.* **13**, 782–785 (2014).
- Bennewitz, R. *et al.* Atomic scale memory at a silicon surface. *Nanotechnology* **13**, 499–502 (2002).
- Crommie, M. F., Lutz, C. P. & Eigler, D. M. Confinement of electrons to quantum corrals on a metal surface. *Science* **262**, 218–220 (1993).
- Heinrich, A. J., Lutz, C. P., Gupta, J. A. & Eigler, D. M. Molecule cascades. *Science* **298**, 1381–1387 (2002).
- Khajetoorians, A. A., Wiebe, J., Chilian, B. & Wiesendanger, R. Realizing all-spin-based logic operations atom by atom. *Science* **332**, 1062–1064 (2011).
- Gomes, K. K., Mar, W., Ko, W., Guinea, F. & Manoharan, H. C. Designer Dirac fermions and topological phases in molecular graphene. *Nature* **483**, 306–310 (2012).
- Ebert, P., Lagally, M. G. & Urban, K. Scanning-tunneling-microscope tip-induced migration of vacancies on GaP(110). *Phys. Rev. Lett.* **70**, 1437–1440 (1993).
- Schuler, B. *et al.* Effect of electron–phonon interaction on the formation of one-dimensional electronic states in coupled Cl vacancies. *Phys. Rev. B* **91**, 235443 (2015).
- Li, Z. *et al.* Lateral manipulation of atomic vacancies in ultrathin insulating films. *ACS Nano* **9**, 5318–5325 (2015).
- Nakakura, C. Y., Zheng, G. & Altman, E. I. Atomic-scale mechanisms of the halogenation of Cu(100). *Surf. Sci.* **401**, 173–184 (1998).
- Huemann, S. *et al.* X-ray diffraction and STM study of reactive surfaces under electrochemical control: Cl and I on Cu(100). *J. Phys. Chem. B* **110**, 24955–24963 (2006).
- Migani, A. & Illas, F. A systematic study of the structure and bonding of halogens on low-index transition metal surfaces. *J. Phys. Chem. B* **110**, 11894–11906 (2006).
- Suleiman, I. A. *et al.* Interaction of chlorine and oxygen with the Cu(100) surface. *J. Phys. Chem. C* **114**, 19048–19054 (2010).
- Celotta, R. J. *et al.* Invited article: autonomous assembly of atomically perfect nanostructures using a scanning tunneling microscope. *Rev. Sci. Instrum.* **85**, 121301 (2014).
- Rademaker, L., Pramudya, Y., Zaanen, J. & Dobrovský, V. Influence of long-range interactions on charge ordering phenomena on a square lattice. *Phys. Rev. E* **88**, 032121 (2013).
- Rost, M. J. *et al.* Scanning probe microscopes go video rate and beyond. *Rev. Sci. Instrum.* **76**, 053710 (2005).
- Feynman, R. P. There's plenty of room at the bottom. *Eng. Sci.* **23**, 22–36 (1960).

Acknowledgements

The authors thank A.J. Heinrich for discussions. This work was supported by the Netherlands Organisation for Scientific Research (NWO/OCW), as part of the Frontiers of Nanoscience program, the Foundation for Fundamental Research on Matter (FOM), and by the Kavli Foundation. J.F.R. and J.L.L. acknowledge financial support by Marie-Curie-ITN grant no. 607904-SPINOGRAPH. J.F.R. acknowledges financial support from MEC-Spain (grant no. FIS2013-47328-C2-2-P) and Generalitat Valenciana (PROMETEO 2012/011).

Author contributions

F.E.K. and E.F. developed the vacancy movement procedure. M.P.R., F.E.K. and A.F.O. programmed the autonomous vacancy manipulation. J.G., M.P.R. and R.T. performed the measurements at 77 K. J.L.L. and J.F.-R. performed the DFT and Monte Carlo calculations. A.F.O. devised the experiment and supervised the research. All authors discussed the results and contributed to writing the manuscript.

Additional information

Supplementary information is available in the [online version of the paper](#). Reprints and permissions information is available online at [www.nature.com/reprints](#). Correspondence and requests for materials should be addressed to A.F.O.

Competing financial interests

The authors have filed a Dutch patent application (NL2016335) for the subject matter described in this manuscript.

Methods

Experimental methods. For most of the results presented here we used an evaporation time of $\tau = 210$ s, resulting in a vacancy coverage of $x = 0.115 \pm 0.004$, where the error is based on the square root of the total number of vacancies counted. Different sample preparations with the same settings gave $x = 0.039 \pm 0.004$ for $\tau = 210$ s, $x = 0.038 \pm 0.004$ for $\tau = 225$ s and $x = 0.17 \pm 0.05$ for $\tau = 240$ s.

To properly study the relation between Cl coverage and evaporation time, one would need a separate means of measuring the evaporation rate (our STM system is not equipped with this).

The Cl-terminated Cu(100) surface seems very inert. The sample used for most of the experiments (with $x = 0.115$) has been in our STM for more than 6 months (at a pressure $p < 10^{-10}$ mbar) without any noticeable degeneration, both in surface appearance and reliability of vacancy manipulation. This suggests that less stringent conditions than ultrahigh vacuum may be acceptable.

Autonomous vacancy manipulation. The procedure for the automatic assembly of vacancy arrays works as follows. First, a marker is built at the top left of the area designated for a 64-bit data block. To define the scan frame, the STM tip locks onto one of the vacancies in the marker, using an atom tracker sequence. Provided that the scan angle and piezo calibrations are fixed, only one marker is needed to fully define the scan frame.

After completing a scan, image recognition is used to identify the positions of all the vacancies in the scan. The initial configuration is compared to the desired final configuration and each vacancy is assigned to a final position by means of the Munkres algorithm²⁷, attempting to minimize the total distance to be traversed. Vacancies are guided to their destinations using an A* pathfinding algorithm²⁸, which prevents vacancies from running into each other or forming dimers.

The computer program keeps a list of assignments that still need to be completed and sends commands to the STM accordingly. Commands include ‘move tip to vacancy at <location>’ and ‘move vacancy into <direction>’. The assignments are based on the current configuration of vacancies as tracked by the program. The STM sends the outcome of each task back to the program. If the STM reports that a vacancy moved in the wrong direction, assignments are recalculated based on the new configuration.

A particular difficulty in the guiding process is to prevent vacancies from blocking each other so that their final position cannot be reached. For this situation we use the following procedure. We identify the vacancies that form a blockage to a specific final position and sort these in order of increasing distance to this position. Next, we move the first vacancy on the list to the final position, the second vacancy to the former position of the first vacancy and so on.

DFT calculations. DFT calculations were carried out with the Quantum Espresso package²⁹, using the PBE exchange correlation functional and PAW pseudopotentials. Relaxation of a unit cell with one Cl and four Cu layers showed that the top layer does not suffer strong deformations. This result did not show an important dependence on the number of Cu layers, remaining unchanged even with only two Cu layers. The structural changes in the presence of a Cl vacancy were calculated in a 3×3 super-cell, allowing full relaxation of the system. The main changes appeared in the position of the Cl atoms, which were pushed towards the site with the missing Cl atom. In comparison, the positions of the Cu atoms barely changed.

The lowest-energy path for a vacancy, shown in Fig. 1b, was calculated in the 3×3 unit cell, moving the position of one of the Cl atoms towards the vacancy, and calculating its energy in every step. In this calculation we constrained the position of all the Cl atoms except the mobile one. The mobile atom had the position in the direction of the vacancy fixed, whereas the other two coordinates were allowed to

relax. The path followed by the Cl atom was above the Cu atom, avoiding becoming closer to other Cl atoms. The energetics of the path did not depend strongly on whether the other atoms were allowed to fully relax or not.

For calculation of the vacancy–vacancy interaction, 5×5 supercells with two Cl vacancies were chosen. The different arrangements of vacancies were calculated, allowing all the Cl atoms to relax. We find that the vacancies have a first-neighbour repulsive interaction, preferring a diagonal arrangement. Qualitative results do not depend on whether the Cu atoms are also allowed to relax. The same calculation with a 4×4 unit cell gave similar results.

Monte Carlo simulations. From the energetics of the DFT calculation for the vacancy–vacancy interaction, we can build a classical lattice gas model defined on the square lattice S . In this model, each site can be either full or empty. For a given configuration, the energy of the system is

$$\mathcal{U} = \sum_{\mathbf{r}, \mathbf{r}' \in S} f(\mathbf{r} - \mathbf{r}') n_{\mathbf{r}} n_{\mathbf{r}'}$$

where $n_{\mathbf{r}}$ is the occupation of site \mathbf{r} (1 for a vacancy, 0 for a filled Cl site). The interaction $f(\mathbf{r}, \mathbf{r}')$ affects every pair of vacancies and its value is taken from the energetics obtained by DFT:

$$f(\mathbf{r} - \mathbf{r}') = \begin{cases} 0.144 & \text{if } \mathbf{r} - \mathbf{r}' \in \{(1, 0), (0, 1), (-1, 0), (0, -1)\} \\ 0.102 & \text{if } \mathbf{r} - \mathbf{r}' \in \{(2, 0), (0, 2), (-2, 0), (0, -2)\} \\ 0.013 & \text{if } \mathbf{r} - \mathbf{r}' \in \{(2, 1), (1, 2), (-2, 1), (1, -2), (2, -1), (-1, 2), (-2, -1), (-1, -2)\} \\ 0.004 & \text{if } \mathbf{r} - \mathbf{r}' \in \{(2, 2), (2, -2), (-2, 2), (-2, -2)\} \\ 0 & \text{otherwise} \end{cases}$$

where the energies are in eV. Using the standard Metropolis update algorithm, we carry out Monte Carlo simulations within the canonical ensemble, that is, with a fixed total number of vacancies, at a given temperature T . The temperature enters in the Metropolis update as the tolerance for accepting a new configuration with higher energy. Starting from an initial random configuration, at every step the update algorithm attempts to move a random vacancy to a random neighbouring filled site. For $T \rightarrow 0$, only new configurations that lower the energy are accepted, so a local energy minimum is finally reached. For $T \rightarrow \infty$, any new configuration is accepted, leading to a fluctuating and disordered state.

Starting from a randomly generated configuration, the Monte Carlo evolution drives the system towards a local free energy minimum. The system develops different domains with stripes in different directions, as observed in the experiment. For the calculations in the main text, a relaxation of 400,000 steps was carried out. Finally, it is worth noting that the results do not change qualitatively if a simpler interaction is assumed:

$$f(\mathbf{r} - \mathbf{r}') = \begin{cases} 0.144 & \text{if } \mathbf{r} - \mathbf{r}' \in \{(1, 0), (0, 1), (-1, 0), (0, -1)\} \\ 0 & \text{otherwise} \end{cases}$$

References

27. Kuhn, H. W. The Hungarian method for the assignment problem. *Nav. Res. Logist. Q.* **2**, 83–97 (1955).
28. Hart, P., Nilsson, N. & Raphael, B. A formal basis for the heuristic determination of minimum cost paths. *IEEE Trans. Syst. Sci. Cybern.* **4**, 100–107 (1968).
29. Giannozzi, P. *et al.* QUANTUM ESPRESSO: a modular and open-source software project for quantum simulations of materials. *J. Phys. Condens. Matter* **21**, 395502 (2009).